Electronic and structural properties of Laves-phase $MgZn_2$ of varying chemical disorder

M. Andersson,[1] M. de Boissieu,[2] S. Brühne,[3] C. Drescher,[3] W. Assmus,[3] S. Ohahshi,[4] A. P. Tsai,[4] M. Mihalkovič,[5] M. Krajčí,[5] and Ö. Rapp[1]

[1]*Material Physics, Kungliga Tekniska Högskolan, 229, 164 40 Kista, Sweden*

[2]*Sciences et Ingénierie des Matériaux et Procédés, INP Grenoble–CNRS–UJF, Rue de la piscine 1130, 38402 St. Martin d'Hères, France*

[3]*Physikalisches Institut, J. W. Göthe-Universität, 60438 Frankfurt am Main, Germany*

[4]*Institute for Multidisciplinary Research of Advanced Materials, Tohoku University, Sendai 980-8577, Japan*

[5]*Institute of Physics, Slovak Academy of Sciences, Dúbravská cesta 9, SK-84511 Bratislava, Slovakia*

(Received 20 January 2010; revised manuscript received 30 April 2010; published 13 July 2010)

The C14 Laves-phase $MgZn_2$ has been investigated from 30 to 36 at. % Mg. In this way chemical disorder can be monitored over a limited concentration range and the influence on electron properties can be investigated. Our studies include thermodynamic calculations of atomic configurations of Mg and Zn at off-stoichiometric compositions, electronic-transport measurements, and electronic band-structure calculations of $MgZn_2$. The disorder introduced by alloying was found to be substitutional for all C14 alloys, and to have a markedly stronger effect on resistivity and magnetoresistance, $\Delta\rho(B)/\rho(0)$, on the Mg-rich side due to strain introduced when Mg substitutes for Zn. $\rho(T)$ and Hall constant were characteristic for weakly disordered binary alloys. $\Delta\rho/\rho$ of $MgZn_2$ was large, reached 6 at 4.2 K and 8 T, and decreased strongly at off-stoichiometric compositions. The results are discussed in view of the band-structure results and in terms of relations between atomic order and electronic properties. Several properties were found to resemble pure Zn. An empirical correlation over more than six orders of magnitude in $\Delta\rho/\rho$ was found for Zn and Zn-based alloys.

DOI: 10.1103/PhysRevB.82.024202 PACS number(s): 72.15.Eb, 72.15.Gd, 61.50.Ah, 71.20.Lp

I. PROBLEM

MgZn-based alloys display a rich variety of intermediate phases of varying structural complexity. Several examples are five binary intermetallic compounds from Mg_2Zn_{11} to Mg_7Zn_3, ternary quasicrystals based on Mg-Zn with addition of about 15 at. % Al,[1,2] or a rare-earth metal,[3] crystalline approximants of these quasicrystals, and also binary amorphous Mg-Zn alloys. Therefore Mg-Zn is a potentially rewarding alloy system for studies of relations between atomic order and physical properties. This approach has rarely been explored for intermetallic compounds, however.

To study the influence of structural order one must be able to control disorder. Structural disorder occurs in a multitude of different forms and cannot be simply quantified in contrast to varying electronic disorder, where $\hbar/\epsilon_F\tau$ can serve as a simple universal parameter. ϵ_F is the Fermi energy and τ the elastic scattering time. Therefore a much simplified case of atomic disorder has been selected, viz., chemical disorder, where changing disorder can be monitored by variation in the concentration within the homogeneity range of a compound.

The simplest one of the various Mg-Zn intermetallic compounds is $MgZn_2$, which is a C14 hexagonal Laves phase with 12 atoms per unit cell. The homogeneity range of this phase, roughly from 30 to 36 at. % Mg, is thus available for variation in chemical disorder. Since the Mg atom is significantly larger than the Zn atom, 1.60 Å and 1.39 Å, respectively, in 12 coordinated metals,[4] one expects this atomic disorder to be different on the Mg- and Zn-rich sides of stoichiometric $MgZn_2$.

In C14 $TiFe_2$ with a similar ratio of the ionic radii of the constituent atoms, it was found from thermodynamic calculations that Ti does not substitute on the smaller Fe sites, but resides on the Ti sublattice, which is made possible by Fe vacancy formation.[5] Our calculations for $MgZn_2$ indicated instead that defects are substitutional on both the Zn-rich and Mg-rich sides of stoichiometric $MgZn_2$. An important factor to make this possible on the Mg-rich side was found to be a compression of the Mg-Zn bond lengths.

We report on results for a series of Mg-Zn alloys in the C14 phase. Properties studied experimentally are the temperature dependence of the electrical resistivity $\rho(T)$, the Hall constant $R_H(T)$, and the field and temperature dependence of the magnetoresistance, $\Delta\rho(B,T)/\rho(0,T)$. Band-structure calculations supplement the results. In Sec II the sample preparation and characterization is described, and the procedures used in experiments and in calculations of thermodynamic properties and band structure are outlined. The transport results are presented in Sec III. $\rho(T)$ and $R_H(T)$ were found to behave normally for simple metallic alloys while $\Delta\rho(B,T)/\rho(0,T)$ displayed large values and a strong concentration dependence. The results from the thermodynamic and band-structure calculations are given in Sec IV. The results are discussed in Sec V. A brief summary is made in Sec VI.

II. SAMPLES AND EXPERIMENTAL AND THEORETICAL TECHNIQUES

A. Experiments

4 samples of C14 Mg-Zn were investigated with Mg concentration in the range 30 to 36 at. %. Phase-diagram investigations have shown that a variation in the composition of the $MgZn_2$ Laves phase could be achieved only in the high-T

region of the phase diagram at about 520 °C in the liquidus area of the phase diagram. Therefore the out of stoichiometry samples have been prepared by an annealing at about this temperature, followed by a quench in order to avoid the eutectic transformation.

Two samples with nominal compositions $Mg_{33}Zn_{67}$ and $Mg_{35}Zn_{65}$ were prepared in Göthe-Universität, (Frankurt). The stoichiometric sample was grown in an Al_2O_3 crucible with the liquid encapsulated top seeded solution technique. During the growing process the melt was covered with a layer of liquid LiCl-KCl. Laue photographs showed that this sample was a single crystal. The 35 at. % Mg sample was grown in a tantalum crucible, heated to 670 °C and cooled by 7.5 °C/h to 545 °C.

Two samples with nominal compositions $Mg_{30}Zn_{70}$ and $Mg_{36}Zn_{64}$ were prepared at IMRAM in Tohoku University (Sendai), by isothermal treatment in the liquidus region followed by quenching. Both samples were kept in the molten state at 700 °C for 3 h, cooled to 520 °C in 120 h, followed by 24 h at 520 °C and quenching. Remaining small amount of liquid was expelled by centrifugation with about 1000 rpm for 20 min. Measured samples were extracted from the bottom of the ingot.

The extension of the phase field of the $MgZn_2$ phase was not known from previous phase-diagram studies. However, possible phases which could form in off-stoichiometric samples are known to be Mg_4Zn_7, Mg_2Zn_{11}, and pure Zn. In the samples prepared we hence systematically looked for these phases using powder x-ray diffraction and scanning electron microscopy (SEM). All samples except the one with 30 at. % Mg, displayed diffraction patterns with a single $MgZn_2$ phase and homogenous SEM images. The 30 at. % Mg sample showed some amount of free Zn, below about 3%, which appeared in grain boundaries.

As mentioned the stoichiometrics sample was a single crystal. The other samples had fairly large grain sizes, >2 mm. The lattice parameters were evaluated by Rietveld refinements for the samples from the Göthe Universität. For the diffraction experiment a $Mg_{32.5}Zn_{67.5}$ sample was studied. In the other measurements single grain $Mg_{33}Zn_{67}$ was investigated. For the 30 and 36 at. % Mg samples the cell parameters were refined by fitting and comparing theoretical, and observed positions of the Bragg peaks using the CELREF software.[6]

The results are shown in Fig. 1. To first approximation the lattice parameters increase linearly with Mg concentration and at similar rates for both cell axes. The high quality of our samples is also supported by the absence of observable peak broadening in the reflections at large Bragg angles. In the 30 and 36 at. % Mg samples the $K\alpha_1$ reflections at $2\theta \approx 70°$ have widths of 0.1° which is about the instrumental resolution.

The preparation techniques in two different laboratories were fairly similar, in particular with a slow cooling from a higher temperature to a temperature above 500 °C. There may nevertheless be differences in grain boundaries and defect configurations in the samples. We discuss if this could mask the effects of varying chemical disorder.

The exact chemical compositions of the samples could not be determined by standard wavelength dispersive analysis in SEM since the variation is not much larger than the accuracy of such measurements. We have thus characterized disorder by the nominal composition. This hypothesis is confirmed by the variations in the lattice parameters, which are almost linear as a function of Mg content. The only error might concern $Mg_{30}Zn_{70}$ for which the actual composition is likely slightly poorer in Zn due to the small amount of Zn precipitates.

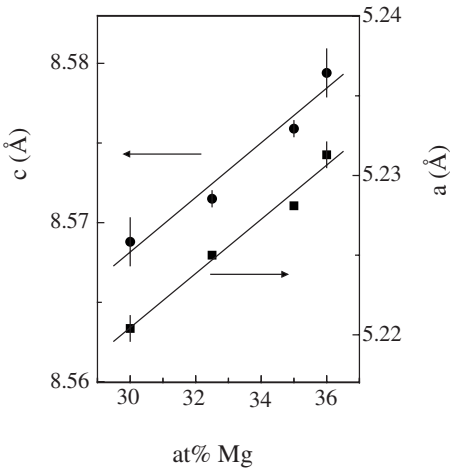

FIG. 1. *a* and *c* lattice parameters of hexagonal C14 Zn-Mg vs Mg concentration. The straight lines show linear regression fits. The bars show estimated errors for the Celref analyses (30 and 36 at. % Mg) and rms errors for the Rietveld refinements (32.5 and 35 at. % Mg). For the *a* axis the errors of the Rietveld analyses are contained within the data symbols.

Zn impurities in the $Mg_{30}Zn_{70}$ sample would lead to enhanced impurity scattering. As discussed in Sec III A this would reinforce our finding, described there, that transport properties are more strongly affected on the Mg-rich side of $MgZn_2$ than on the Zn-rich side. Differences in grain-boundary configurations are not an issue. The grains are very much larger than the electron mean-free path and grain-boundary scattering is a minor contribution to the resistivity. We conclude that variation in chemical order is the main source of variation in sample properties.

Electrical measurements were made with standard dc techniques. Contacts of silver paint were used with four contacts for the resistivity measurements and five for the Hall measurements. The Hall field E_H was measured in magnetic fields, generally up to 8 T, and in some cases to 12 T. Errors in absolute values for the resistivity and the Hall measurements were estimated to be below 15% and mainly due to errors in the sample dimensions. The accuracy of the magnetoresistance measurements was generally of the order of a few times 10^{-5} in $\Delta\rho/\rho$.

B. Calculations

To evaluate energetics of compositional variation on the Zn- and Mg-rich sides respectively, we have combined calculations with the Vienna *ab initio* simulation package (VASP) (Refs. 7 and 8) of the internal energy at $T=0$ K in a $2\times2\times2$ supercell holding 95/96 atoms, with the embedded

atom potential calculations of the phonon densities of states[9] by diagonalization of the dynamical matrix. Finally, we made simple estimates (without correlations beyond the supercell) of the chemical mixing entropy.

The VASP calculations were performed with a semilocal exchange-correlation functional in the general gradient approximation (GGA).[10] Within the last decade the projector-augmented-wave- (PAW-) GGA functional used by us or other similar functionals are generally accepted as standard and superior to (older) local density approximations. In the past we have used the PAW-GGA functional for evaluation of hundreds of binary and ternary alloy systems[11] with remarkable realism (including the Mg-Zn system), which further supports this choice.

The calculations were converged to $7\times7\times4$ **k**-point meshes, giving 48 independent **k** points inside the Brillouin zone (95/96 atoms per cell): This was about the limit of our computational resources. The computed internal energies after full relaxation of atomic positions as well as cell shape/volume, were taken relative to the tie-line between the energies of $MgZn_2$ and the neighboring stoichiometric compounds Mg_4Zn_7 (Pearson symbol mC110) on the Mg-rich side and Mg_2Zn_{11} (Pearson symbol cP39) on the Zn-rich side.

For estimating entropic effects, we have worked with embedded atom potentials fitted to VASP data used in a recent combination of experimental and computational phonon studies of $MgZn_2$.[9] The supercell shape/volume obtained from VASP optimization was used and the vibrational energy F_{vib} was calculated from the expression

$$F_{vib} = k_B T \int d\omega \left\{ D(\omega) + \ln\left[2 + \sinh\left(\frac{\hbar\omega}{k_b T} \right) \right] \right\} \qquad (1)$$

with the phonon density of states $D(\omega)$ obtained in the calculations.

The electronic-structure calculations are based on the density-functional theory. For the structural relaxation and total energy calculations we have used the VASP package.[7,8] For the density of states (DOSs) and the band structure of the structurally optimized system we used the linear-muffin-tin orbitals (LMTOs) method.[12,13] With this method a very fine sampling of the Brillouin zone can be obtained.

III. EXPERIMENTAL RESULTS

A. Resistivity and Hall effect

The results for the electrical resistivity $\rho(T)$ are shown in Fig. 2 from 4 K to room temperature. The overall behavior is typical for simple metallic alloys with an almost flat $\rho(T)$ below about 20 K and an increase with temperature which is almost linear above 100 K. The displacement of the curves is characteristic for weakly increasing electronic disorder with deviations from the stoichiometric composition. However, with increased electronic disorder one usually observes a decrease in $d\rho/dT$, and eventually a sign change, while in this case $d\rho/dT$ instead increases substantially with electronic disorder on the Mg-rich side.

The resistivity ratio $r=\rho(295\ \mathrm{K})/\rho(4.2\ \mathrm{K})$ at stoichiometric composition was 44, which is a large value for an intermetallic compound of a moderately complex structure. This indicates high sample quality. The inset illustrates that r decreased for off-stoichiometric compositions and more strongly so on the Mg-rich side. Thus, a similar change in Mg concentration gives a stronger contribution to electronic disorder on the Mg-rich side. Likely this is due to the strain introduced when Mg ions occupy Zn sites.

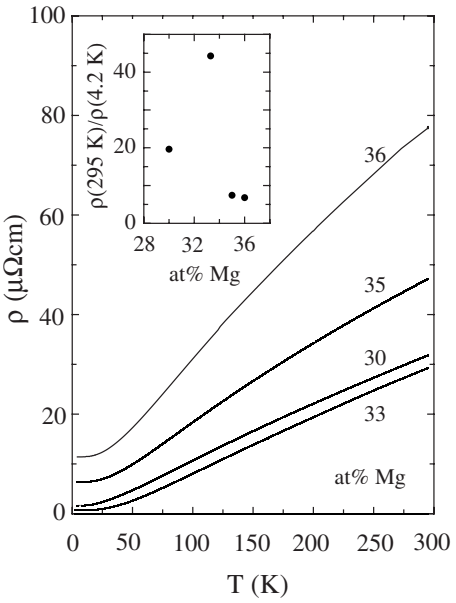

FIG. 2. Resistivity, $\rho(T)$, vs temperature for four C14 Mg-Zn samples. The resistivity increase is more prominent on the Mg-rich side than on the Zn-rich side of $Mg_{33}Zn_{67}$. Inset: the resistance ratio vs Mg concentration.

Zn impurities in the 30 at. % Mg sample do not question this conclusion. The closely parallel curves of $\rho(T)$ at 33 and 30 at. % in Fig. 2 indicate that phonon scattering is similar and hence that temperature-dependent properties would not be affected. If Zn impurities have contributed to temperature-independent scattering in $Mg_{30}Zn_{70}$ the observed $\rho(4.2\ \mathrm{K})$ is larger and r smaller than for a sample without Zn impurities. The conclusion that properties are more strongly affected on the Mg-rich side than on the Zn-rich side would then be reinforced.

The Hall field E_H was linear in magnetic field up to 8 T at all measured temperatures and the Hall constant R_H was evaluated from the slope of straight lines fitted to these data. Results for R_H are shown in Fig. 3. If one estimates R_H from $-1/ne$ with 24 free charge carriers per unit cell one finds $|R_H| \approx 5\times10^{-11}\ \mathrm{m^3/As}$, much smaller than the values in Fig. 3. However, when taking into account that nine Brillouin zones of $MgZn_2$ are filled and five zones have partial charge occupancy,[14] the number of mobile charge carriers per unit cell is reduced to 6. The corresponding free electron $|R_H| \approx 0.2\times10^{-9}\ \mathrm{m^3/As}$. The experimental R_H is larger, indicating that the effective number of charge carriers is further reduced. This presumably arises due to a mixture of holelike and electronlike Fermi surfaces in the remaining five bands.

Within measurement errors R_H was almost independent of Mg concentration for $T \geq 100$ K. For the 36 at. % Mg sample this is barely fulfilled. At lower temperatures R_H in-

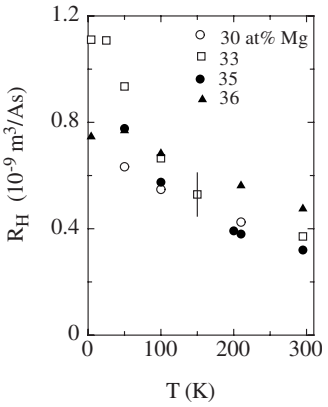

FIG. 3. Hall coefficient $R_H(T)$ for C14 Mg-Zn samples. An estimated measurement error of 15% is shown for one sample.

creased more strongly with decreasing temperature for $MgZn_2$ than for the other samples. At $T \geq 100$ K the results indicate that the compensation, $n_{hole}/n_{el.}$, is not sensitive to varying Mg concentration and has a similar temperature dependence for all samples. The temperature dependence qualitatively resembles pure polycrystalline Zn where R_H at 297 K was found to be about 6 10^{-11} m^3/As and roughly a factor of two larger at 77 K.[15]

B. Magnetoresistance of stoichiometric $MgZn_2$

The temperature dependence of the magnetoresistance $\Delta\rho(B,T)/\rho(0,T)$ for the stoichiometric sample is shown in Fig. 4 for two orientations of current and field. For $\mathbf{B} \perp \mathbf{j}$ and sample plane the magnetoresistance was large and reached above 6 at 8 T and 4.2 K (panel a). For $\mathbf{B} \| \mathbf{j}$, $\Delta\rho/\rho$ was more than an order of magnitude smaller at 4 K (panel b). A tendency of saturation in $\Delta\rho/\rho$ was observed for $T \leq 50$ K when $\mathbf{B} \| \mathbf{j}$. The magnetoresistance decreased strongly with increasing temperature for both field directions.

The Laves phases are topologically close packed and a strong anisotropy of physical properties is not expected. The angular dependence of $\Delta\rho/\rho$ is shown in Fig. 5 with the sample rotated from the direction $\mathbf{B} \perp \mathbf{j}$ and sample plane to $\mathbf{B} \| \mathbf{j}$ in the plane. $\Delta\rho/\rho$ in Fig. 5 is sinusoidal-like, suggesting that its dependence on orientation of $\mathbf{j}$ and $\mathbf{B}$ is due to a Lorentz force $\mathbf{j} \times \mathbf{B}$.

Large effects on the magnetoresistance are expected when the electrons are able to execute several turns around the magnetic field axis without scattering during a relaxation time τ. With the cyclotron frequency $\omega_c = eB/m^*$ this condition implies $\omega_c \tau \gg 1$.

$\omega_c \tau$ can be estimated from

$$\omega_c \tau = \frac{B|R_H|}{\rho} \tag{2}$$

by using essentially the free electron estimates of $\rho = m^*/n^* e^2 \tau$ and the Hall constant $R_H = -1/n^* e$. We note, however, that τ, the least known parameter in Eq. (2), has been eliminated. With R_H at most $\approx 10^{-9}$ m^3/As from Fig. 3 and the smallest value of $\rho(T) = 0.7$ $\mu\Omega$ cm for $MgZn_2$ at 4.2 K

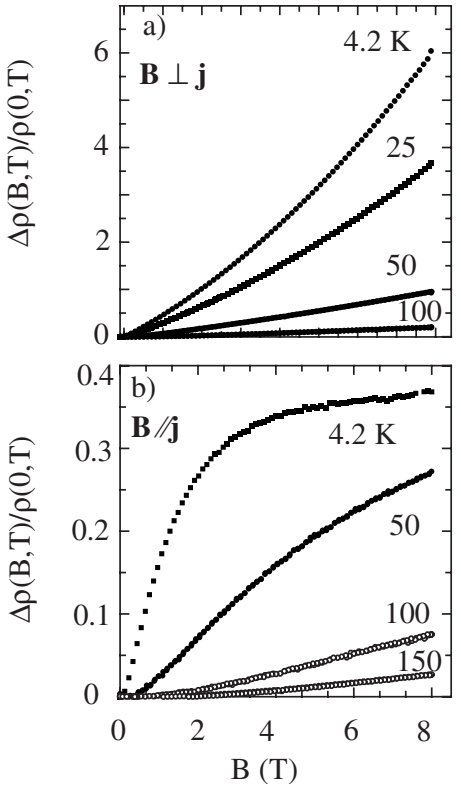

FIG. 4. Magnetoresistance for the stoichiometric sample vs magnetic field at the temperatures indicated (in Kelvin). Panel (a): transverse magnetoresistance and panel (b): longitudinal.

from Fig. 2 one finds $\omega_c \tau \leq 1.1$ The large magnetoresistance is therefore remarkable.

In the derivation of Eq. (2) it was implicitly assumed that the charge-carrier densities in R_H and ρ were the same and hence cancelled. However, both holes and electrons contribute to the conductivity but oppose each other in the Hall effect. The effective charge densities n^* in ρ and R_H, are thus expected to be different and the right hand member of Eq. (2) should be multiplied by the ratio of the effective charge densities n^*_{Hall}/n^*_{res}. This correction further reduces the estimate of $\omega_c \tau$. We conclude that $\omega_c \tau \lesssim 1$ for all studied samples, temperatures, and fields.

The magnetoresistance is frequently analyzed by Kohler plots.[16] In semiclassical transport theory $\Delta\rho/\rho$ depends only

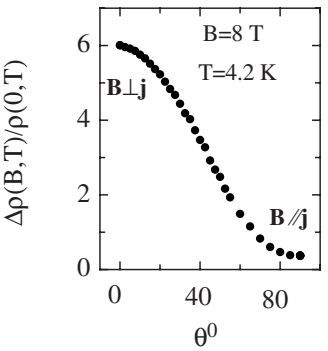

FIG. 5. Magnetoresistance for $MgZn_2$ at 4.2 K and 8 T at varying angles θ between $\mathbf{B}$ and $\mathbf{j}$.

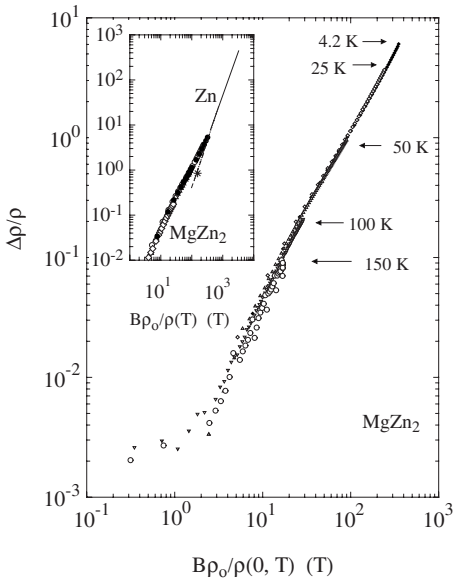

FIG. 6. The magnetoresistance of $MgZn_2$ vs a normalized magnetic field, where $\rho_o=\rho(295\ \mathrm{K})$. Data are in the range $4.2\leq T\leq 150$ K, $B\leq 8$ T. Arrows show the maximum $\Delta\rho/\rho$ at the temperatures indicated. Inset: present data for $\Delta\rho/\rho>1\%$ together with data for pure Zn of unspecified purity (Ref. 16). The * is Kapitzas most pure Zn sample (Ref. 17) at 30 T and 77 K. The dashed line extrapolates the data of Ref. 16.

on the product $B\tau$, where the relaxation time $\tau(T)\sim 1/\rho(T)$. Hence, when alloy systems of similar charge densities and effective masses are studied, one expects $\Delta\rho/\rho\sim f[B/\rho(T)]$ to be a universal function. It is convenient to normalize $\rho(T)$ with a resistivity at a given temperature, say ρ_o. The argument of f is then a scaled magnetic field. Kohlers expression reads

$$\frac{\Delta\rho}{\rho}=f\left[\frac{B\rho_o}{\rho(0,T)}\right]. \tag{3}$$

This function is shown in the main panel of Fig. 6 with the data of Fig. 4(a) and with results at $T=150$ K added. Up to 100 K the fit to Eq. (3) is excellent with minor deviations noticeable at 150 K. The range of this fit of $\Delta\rho/\rho$ over three orders of magnitude is among the largest observed for the magnetoresistance of pure metals and compounds.

The straight line in the inset of Fig. 6 shows results for pure Zn from a collection of magnetoresistance results for pure metals,[16] together with the data from Fig. 4 for $\Delta\rho/\rho>1\%$. We have not been able to find information on the purity of this Zn sample. These data are discussed in Sec. V.

For pure Zn, ρ_o in Eq. (3) was taken to be the value at the Debye temperature, Θ_D. However, Θ_D for Zn and $MgZn_2$ are both close to 330 K,[18] rather similar to the present choice of 295 K, and the corresponding correction has been neglected.

The pure Zn data obey $\Delta\rho/\rho\sim[B\rho_o/\rho(T)]^\alpha$ with α close to 2. This result is expected in a free electron model for a divalent metal with equal number of electrons and holes in two unfilled bands.[19] For $MgZn_2$, α is smaller, ≈ 1.4 and does not show signs of saturation up to 8 T. Within a two band free electron model this indicates deviations from full

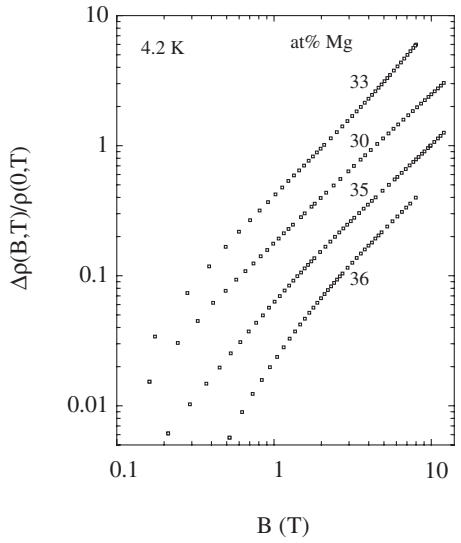

FIG. 7. The magnetoresistance for C14 Mg-Zn at 4.2 K vs magnetic field at various magnesium concentrations.

compensation. However, such a model,[19] is not compatible with the presently observed magnitude of $\Delta\rho/\rho$ and the small values of $\omega_c\tau$ estimated for our sample.

C. Concentration dependence of the magnetoresistance

Another prominent feature of the magnetoresistance is the strong concentration dependence. As shown in Fig. 7, $\Delta\rho(B,T)/\rho(0,T)$ is reduced by somewhat more than a factor of 2 for each step in the sequence 33, 30, 35, and 36 at. % Mg. This change is again stronger on the Mg-rich side than on the Zn-rich side.

At off stoichiometric compositions Kohlers rule fails for all alloys studied. This is illustrated in Fig. 8 for $Mg_{36}Zn_{64}$. Clearly the small concentration change from the stoichiometric composition causes significant changes in details in the band structure. Band-structure calculations were undertaken in order to elucidate this behavior.

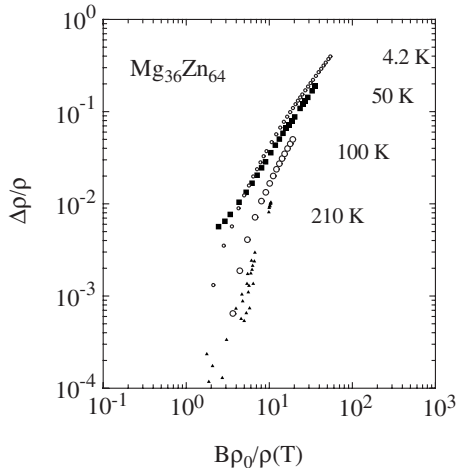

FIG. 8. The magnetoresistance of the $Mg_{36}Zn_{64}$ sample plotted in the same way as in Fig. 6. Here Kohlers rule fails.

TABLE I. Energetics of structural variations around C14 $MgZn_2$. E_0 is the internal energy, F_{vib} the vibrational free energy at 790 K, F_{mix} is the chemical mixing entropy at the same temperature, computed as $k_BT \ln W$. Site multiplicities are $W=16$ for Zn 1, $W=48$ for Zn2, and $W=32$ for Mg. Zn1 and Zn2 are the two Zn sites in the C14 structure.

Config.	x (at. % Mg)	E_o (eV)	F_{vib} (eV)	F_{mix} (eV)	F (eV)
$MgZn_2$	33.3	0	0	0	0
Mg at Zn2	34.4	0.134	−0.010	−0.263	−0.139
Vac at Zn2	33.7	0.202	0.333	−0.263	0.272
Zn at Mg	32.3	0.230	−0.605	−0.236	−0.611
Mg at Zn1	34.4	0.250	0.355	−0.189	0.416
Vac at Zn1	33.7	0.442	0.133	−0.189	0.386

IV. RESULTS OF THE CALCULATIONS

A. Thermodynamic calculations

The energies for different configurations of the additional or missing atoms at off-stoichiometric compositions were calculated by substitution of a single atom in a stoichiometric $MgZn_2$ $2\times2\times2$ supercell. The results are shown in Table I. Zn1 and Zn2 are the two nonequivalent Zn sites in the C14 phase.

The energy E_0 in Table I is related to the tie-lines connecting stable structures of the energy-composition Mg-Zn diagram. These energies are hence relative to $MgZn_2$-Mg_2Zn_{11} or $MgZn_2$-Mg_4Zn_7 so we have accurately evaluated total energies for all of these structures. The mixing enthalpy (not quoted in Table I) is about −0.14 eV/atom for all variant models, including the stoichiometric structure.

The standard way to estimate volume available to an atom is the Voronoi construction. The "large" Mg site has 19.2 Å^3, and the two Zn sites have $V_{voro}=15.80$ Å^3 and 15.65 Å^3 for Zn1 and Zn2, respectively. This is for the stoichiometric structure. Of course atomic positions relax in the $2\times2\times2$ supercell upon the substitutions and the Voronoi volumes are adjusted to the sites of an atom.

One would naively expect that the Zn sites are too tight for the Mg atom. However, the lowest energy cost on the Mg-rich side was found for Mg substitution on the Zn2 site and not by Zn vacancy formation as expected. These results are rather counterintuitive.

Mg has a similar coordination on both Zn1 and Zn2 sites. It is surrounded by six Zn and six other Mg atoms, and Mg-Zn bond lengths after VASP relaxation are nearly the same, 2.6–2.7 Å, to be compared with 3.03 Å in stoichiometric $MgZn_2$. We found a considerable energetic difference for Mg substituting on Zn2 and Zn1 of ≈0.5 eV. The corresponding coordination shells differ mainly by the spatial arrangement of atoms, (while radial bond lengths are practically identical). A prominent feature in Fig. 9 is that the six surrounding Mg atoms in panel a) form an almost planar hexagon, which in panel b) has become strongly corrugated.

The importance of vibrational entropic terms should also be pointed out. For example, in the case of Zn substituting on the Mg site this is the strongest energetic term, which stabilizes the $MgZn_2$ compound on the Zn-rich side.

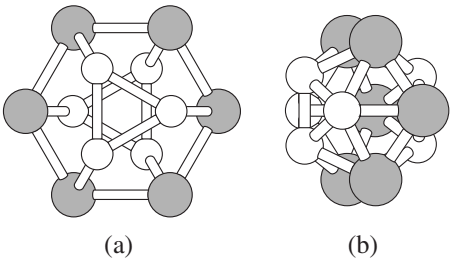

FIG. 9. Atomic environments (after VASP relaxation) around a substituted Mg atom on (a): a Zn1 site and (b): on a Zn2 site. Panel (b) has been rotated by 90° around a vertical axis in the plane of the figure. (Mg atoms are gray.)

B. Electronic band structure

C14 $MgZn_2$ has space group No. 194 with 12 atoms in the hexagonal unit cell. Figure 10 shows the DOS calculated for the lattice parameters $a=5.225$ Å and $c=8.5715$ Å.

The changes in the lattice parameters in the C14 phase are of order ±0.1% around the stoichiometric composition, (Fig. 1). These changes in the lattice parameters have only a minimal effect on the electronic structure and in a first approximation their influence on the DOS can be neglected. The width of the band is 9.83 eV, somewhat smaller than that of pure Zn (10.65 eV). Near the bottom of the band at around −8 eV, the Zn d band is located. The Fermi energy falls into a small local minimum.

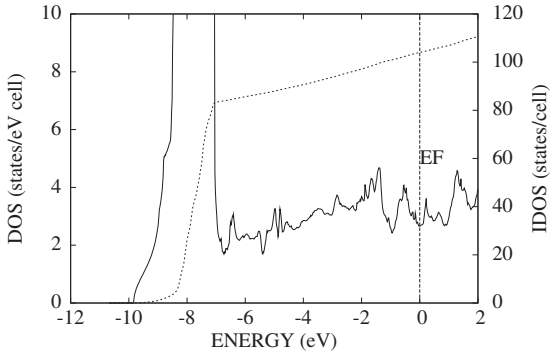

FIG. 10. The DOS of the $MgZn_2$ compound. The dotted curve shows the integrated DOS (IDOS, right-hand-side scale). It cuts the Fermi energy at 104 electrons/cell.

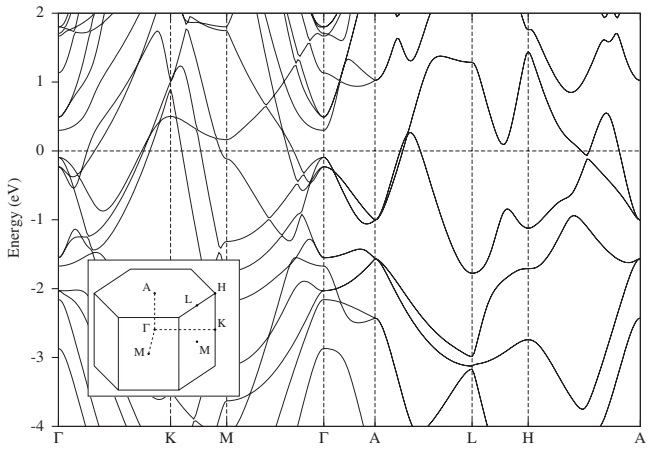

FIG. 11. The band-structure $E_n(\mathbf{k})$ between high symmetry points in the Brillouin zone in the vicinity of −4 to 2 eV around the Fermi level. Inset: the Brillouin zone with some symmetry points marked.

The calculated result for DOS at the Fermi level of $MgZn_2$ is 0.221 states/(eV atom). This can be compared with experimental results for the electron specific heat γ of 0.694 mJ/mole,[18] corresponding to a DOS of 0.29 states/(eV atom). The electron effective mass is enhanced, however, by a factor $1+\lambda$, where λ is the electron-phonon interaction parameter. From the observed superconducting T_c of 0.9 K,[20] and the Debye temperature of 330 K,[18] and taking a conventional value of the Coulomb repulsion parameter of 0.1, one then finds from McMillan's T_c formula[21] that $1+\lambda=1.38$. The experimental DOS at ϵ_F is thus 0.21 states/(eV atom) in good agreement with the (bare) calculated value.

Both Mg and Zn are divalent metals. One could assume that at least in an approximation of the rigid-band model the substitutional defects should not lead to a change of the DOS around the Fermi level and therefore the electronic properties of $MgZn_2$ should not be sensitive to chemical disorder. However, the situation is more complex. The Mg substitution by the smaller Zn atom or vice versa will lead to a substantial local deformation of the lattice and therefore one cannot assume that the shape of the band remains rigid.

Electronic properties of crystals with small unit cells are usually discussed within the semiclassical Bloch-Boltzmann theory, where the dispersion of the bands, $E_n(\mathbf{k})$ plays an essential role. For an understanding of the sensitivity of the electronic properties to small chemical disorder the picture of the band structure in the reciprocal space can be helpful. Figure 11 presents the band structure $E_n(\mathbf{k})$ in the Brillouin zone in the vicinity from −4 to 2 eV around the Fermi level. The figure demonstrates that the Fermi surface should have a very complex shape consisting of many pieces. Interesting parts of the band structure are the paths between the high symmetry points A, L, and H, showing dispersion of the bands at the hexagonal faces of the first Brillouin zone. The dispersion of the bands along AL and AH indicates that the Fermi surface should have pockets at (or near) these faces consisting of holes and electron carriers. In a model of two bands (electrons and holes) the contribution to the magnetoresistance is proportional to B^2 for small fields and saturates in strong magnetic fields if the compensation between electrons and holes deviates from 1.

The disorder breaks the exact periodicity of the system. If the same defect is periodically repeated in all unit cells then one can expect a small shift in the bands with respect to the Fermi energy. The system with a random distribution of the defects can be analyzed using perturbation theory. In this formalism the effects of disorder on the bands is to smear them out. The disorder will also lead to a nonzero residual resistivity of the system observed in Fig. 2. An important contribution to the magnetoresistance may also come from the open orbits. A failure of the magnetoresistance to saturate in strong fields could indicate that the Fermi surface can support open orbits. In the present case this interpretation does not seem likely however since the angular dependence in Fig. 5 is a smooth function of the angle between **B** and **j** without peaks and moreover since $\omega_c\tau$ is small enough that electrons would not have enough time to display such features.

V. DISCUSSION

Three noteworthy results are discussed; substitution of Mg on Zn sites, the similarity to the electronic properties of pure Zn, and the strong concentration dependence of the magnetoresistance.

A. Substitutional defects

One surprising part of our study is that excess Mg substitutes on Zn sites and furthermore, that this occurs mainly at only one of the two Zn sites, i.e., Zn2. As mentioned, this substitution was not expected due to the large difference in atomic radii of Mg and Zn. The shrinking in bond lengths which makes this possible is substantial, and of order 10–13 %. As a consequence the 16-fold coordination in $MgZn_2$ shrinks to 12-fold for the Mg-rich samples.[22]

The distinction between Zn1 and Zn2 sites is more subtle. The Zn1 environment is symmetric with surrounding Mg atoms forming a nearly flat hexagon. Zn2 is less symmetric, and although the Mg hexagons remain they have become strongly distorted, thus indicating stronger atomic disorder.

Mg substitution on Zn sites is supported by our results for the lattice parameters since the rate of change in a and c with Mg concentration in Fig. 1 is equally strong on both sides of the stoichiometric composition. This would not be expected in a model where excess Mg is on Mg sites and additional Zn vacancies are created. The stronger sensitivity of the resistivity and the magnetoresistance to concentration changes on the Mg-rich side is also consistent with the stronger atomic disorder in Mg-rich samples.

B. Similarity to electronic properties of pure Zn

It is interesting to note that several electronic properties of $MgZn_2$ are similar to those of pure Zn. Our calculation of the DOS of hcp Zn has a quite similar shape as the DOS of $MgZn_2$ in Fig. 10, except for a stronger modulation by van Hove singularities in $MgZn_2$, which results from the more complex structure. Also in pure Zn there is a dominant d

TABLE II. Some electronic properties of Zn and Zn alloys. *a* indicates amorphous, *i* icosahedral. State is a brief characteristic of sample order/disorder; e.g., at-o, el-dis means electronic order and atomic disorder. $|\Delta\rho/\rho|^{max}$ is the largest observed magnetoresistance.

Alloy	State	$\rho_{4\ K}$ ($\mu\Omega$ cm)	$\rho_{295\ K}/\rho_{4\ K}$	$\lvert\Delta\rho/\rho\rvert^{max}$	Ref.
a-$Mg_{67}Zn_{33}$	at-dis, el-dis	50	0.97	$2\ 10^{-4}$	25 and 26
i-$Zn_{60}Mg_{30}Ho_{10}$	at-o, el-dis	220	0.95	$4\ 10^{-3}$	27
$MgZn_2$	at-o, el-o	0.67	44	6	This work
Zn	at-o, el-o	$5\ 10^{-3} \pm 50\%$	$1000 \pm 50\%$	500	16

band at the bottom of the band and essentially paraboliclike *sp* bands. The pseudogap at ϵ_F is more pronounced in Zn and the DOS at ϵ_F is 0.199 compared to 0.221 states/(eV atom) for $MgZn_2$.

Furthermore, the Debye temperatures of Zn and $MgZn_2$ differ by only 1%.[18] The superconducting transition temperature T_c is 0.86 K for Zn and 0.91 K for $MgZn_2$.[20] Therefore the electron-phonon interaction is also quite similar with a difference in electron-phonon interaction parameter λ of below 1%. The electronic specific-heat coefficients γ differ by about 6%.[18] The notable exceptions in the present results to this similarity with pure Zn are the significantly larger ρ and R_H for $MgZn_2$. The larger ρ is related to a larger scattering rate due to disorder, and R_H is quite sensitive to details of the band shapes and to the balance between electrons and holes.

The inset of Fig. 6 suggests that also the magnetoresistance of $MgZn_2$ behaves similarly to pure Zn. At the lowest temperature in Kapitzas data, 77 K, ρ_o/ρ for the most pure Zn sample was 5.3.[17] This value is in good agreement with the value for pure Zn compiled by Meaden.[23] Hence $\rho_{295\ K}/\rho_{4\ K}$ of Kapitzas most pure Zn sample can be expected to be similar to that of Meaden's sample, which was 1000. We therefore assume that the Zn data quoted by Kohler[16] have a similar resistance ratio and allow for a significant error in this estimate by taking $\rho_{295\ K}/\rho_{4\ K} = 1000 \pm 50\%$ for the pure Zn data in the inset of Fig. 6. The maximum of $\omega_c\tau$ would then be in the range 5–10 depending on the choice of R_H at low temperatures of 0.1×10^{-9} m^3/As (Ref. 15) or 0.2×10^{-9} m^3/As.[24] Thus, for pure Zn, electrons can make several turns around the magnetic field axis without scattering. Neglecting the difference in slopes in the inset of Fig. 6 one can qualitatively see the decrease of $\Delta\rho/\rho$ with decreasing $B\rho_o/\rho(T)$ in Fig. 6 as mainly due to an increased scattering rate.

There is thus a predominance of Zn-like electronic properties in $MgZn_2$. This is particularly suggestive for the magnetoresistance in the inset of Fig. 6, where the correlation qualitatively extends over more than four orders of magnitude in the magnetoresistance. One may therefore conjecture that $MgZn_2$ behaves as "generalized" Zn where the properties which can be conveniently accessed have been extended by diluting the Zn concentration and increasing the scattering rate.

One can compare the magnetoresistance of Zn and some Zn alloys in the limits of poor and good atomic and electronic order. A few Zn alloys have been selected in Table II. $Mg_{30}Zn_{60}Ho_{10}$ has the same ratio of Mg/Zn concentration as $MgZn_2$ but 10 at. % of Ho changes structure and properties dramatically. Amorphous Mg-Zn alloys can only be produced in the Mg-rich end of the phase diagram. The magnetoresistance of this alloy is negative and positive for the others. Here we are interested mainly in the magnitude of $\Delta\rho/\rho$.

The examples in Table II have been arranged in order of increasing maximum of the observed magnetoresistance. This is also the order of increased atomic order in the sense of symmetry and few impurities. For the quasicrystal, $\rho_{4\ K}$ does not decrease in the same sequence as atomic order increases in Table II since in quasicrystals atomic order and electronic disorder is often combined. Weak localization in atomically ordered quasicrystals are well known and the coordinates $[\rho_{4\ K}, \Delta\rho/\rho^{max}]$ of icosahedral $Mg_{30}Zn_{60}Ho_{10}$ fit into a general correlation for the magnetoresistance in weak electronic disorder.[28]

Table II illustrates that the magnetoresistance of Zn alloys (with the exception of quasicrystals) increases with atomic order. In this sense the result for $MgZn_2$ falls in line with the other results and the magnitude would perhaps not be surprising. However, the problem why $\omega_c\tau$ is so small for $MgZn_2$ and how this is consistent with a large magnetoresistance is left open.

C. Concentration dependence of the magnetoresistance

Experimentally the strong sensitivity of the magnetoresistance to variations in the Mg concentration is evidenced both by the significant changes in the magnitude (Fig. 7) and the rapid change from an excellent fit to Kohlers rule for $MgZn_2$ to break down for small changes of the Mg concentration. (Fig. 8).

This can be due to changes in the shape of the Fermi surface or a change in the anisotropy of the scattering time. Our calculations have shown that a modest chemical disorder can lead to significant changes in the electronic properties. The experimentally observed sensitivity of the magnetoresistance to small chemical disorder is in agreement with the complexity of the electronic structure of the $MgZn_2$ compound.

The change in atomic order in off-stoichiometric $MgZn_2$ can be compared to changes of atomic order in Zn-related samples over a wide range of varying order. The results are shown in Fig. 12. The abscissa can in general be taken as a measure of atomic order. However, this is not the case for quasicrystals and this sample from Table II has been omitted. Figure 12 shows that the strong decrease in the magnetore-

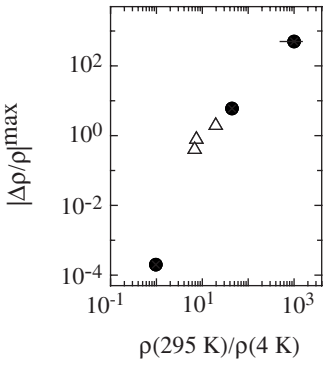

FIG. 12. The maximum of the observed magnetoresistance vs resistance ratio $\rho(295\ \mathrm{K})/\rho(4\ \mathrm{K})$. ●: samples from Table II and △: off-stoichiometric $MgZn_2$.

sistance for off-stoichiometric samples is qualitatively in line with a relation between $\rho_{295\ \mathrm{K}}/\rho_{4\ \mathrm{K}}$ and $\Delta\rho/\rho$ over a wide range extending over more than 6 orders of magnitude in $\Delta\rho/\rho$.

From right to left in Fig. 12 the different forms of atomic order and disorder are: (i) residual impurities in the clean limit, (ii) decrease in the lattice symmetry in C14 $MgZn_2$, (iii) introduction of defects and strain in C14 Mg-Zn at off-stoichiometric compositions, and (iv) loss of the lattice in the disordered limit. It is interesting to note that the effects on a physical property of these different types of atomic order can be qualitatively measured by the single simple parameter $\rho_{295\ \mathrm{K}}/\rho_{4\ \mathrm{K}}$.

VI. BRIEF SUMMARY

Mg-Zn alloys have been studied over the range from 30 to 36 at. % Mg where the C14 hexagonal Laves phase can be formed. For Mg-rich alloys, the larger Mg-ion substitutes on the Zn2 site. This was found to be possible due to contraction of the first coordination shell and the Mg-Zn bond length.

The Hall constant was nearly independent of variations in Mg concentration at $T \geq 100$ K. $\rho(T)$ increased with deviations from stoichiometric compositions as expected for impurities in alloys. For stoichiometric $MgZn_2$ the magnetoresistance reached the large value of 6 at 4 K and 8 T. This value decreased strongly when the Mg concentration deviated from the stoichiometric composition. The large values of $\Delta\rho/\rho$ are surprising in view of the estimate of $\omega_c\tau$ of $\lesssim 1$.

The electrical resistivity and the magnetoresistance were found to vary more strongly with Mg concentration on the Mg-rich side than on the Zn-rich side of stoichiometry. This could be traced to (i) the strong disorder and strain introduced when substituting Zn by Mg on the Mg rich side, and (ii) the indications from band-structure calculations that certain parts of the complex Fermi surface will be significantly influenced by small changes in chemical disorder.

The band-structure calculations also indicated that electron bands at the hexagonal faces of the Brillouin zone contain parts of small electron and hole pockets so that properties can change rapidly with changing concentration. This is illustrated by the dramatic break down of Kohler' s rule at off-stoichiometric compositions.

The electronic properties of $MgZn_2$ in many respect resemble those of pure Zn. In particular, the magnitude of the magnetoresistance and its sensitivity to varying Mg concentration, were found to be consistent with the corresponding properties for Zn and Zn alloys over a wide range from atomically well ordered to disordered samples.

ACKNOWLEDGMENTS

This work has been supported by the European Network of Excellence on Complex Metallic Alloys supported by EU under Contract No. NMP-CT-2005-500140. We thank Charles Maragna for help with the initial experiments. M.M. and M.K. thank also for support from the Grant Agency for Science of Slovakia (Grant No. 2/5096/25) and from the Slovak Research and Development Agency (Grant No. APVV-0413-06, CEX-Nanosmart).

[1] P. Ramachandrarao and G. V. S. Sastry, Pramana **25**, L225 (1985).
[2] T. Takeuchi and U. Mizutani, Phys. Rev. B **52**, 9300 (1995).
[3] Z. Luo, S. Zhang, Y. Tang, and D. Zhao, Scr. Metall. Mater. **28**, 1513 (1993).
[4] W. B. Pearson, *Crystal Chemistry and Physics of Metal and Alloys* (Wiley, New York, 1972).
[5] K. C. H. Kumar and I. Delaey, CALPHAD: Comput. Coupling Phase Diagrams Thermochem. **18**, 223 (1994).
[6] J. Laugier and B. Bochu, Laboratoire des Matèriaux et du Gènie Physique, Technical Report No. BP 46, 1999 (unpublished). See also: http://www.inpg.fr/LMPG and http://www.ccp14.ac.uk/tutorial/lmgp/
[7] G. Kresse and J. Furthmüller, Phys. Rev. B **54**, 11169 (1996).
[8] G. Kresse and D. Joubert, Phys. Rev. B **59**, 1758 (1999).
[9] P. Brommer, M. de Boissieu, H. Euchner, S. Francoual, F. Gähler, M. Johnson, K. Parlinski, and K. Schmalzl, Z. Kristallogr. **224**, 97 (2009).
[10] J. J. Perdew and Y. Wang, Phys. Rev. B **45**, 13244 (1992).
[11] M. Widom, M. Mihalkovič, and collaborators, see http:\\alloy.phys.emu.edu
[12] O. K. Andersen, Phys. Rev. B **12**, 3060 (1975).
[13] H. L. Skriver, *The LMTO Method* (Springer, Berlin, 1984).
[14] P. Rennert and M. Taut, Phys. Status Solidi **41**, 703 (1970).
[15] G. S. Lane, A. Huglin, and J. Stringer, Phys. Rev. **135**, A1060 (1964).
[16] M. Kohler, Annalen der Physik, Folge 6, Vol. **6**, 18 (1949).
[17] P. Kapitza, Proc. R. Soc. London, Ser. A **123**, 292 (1929).
[18] M. Morishita and K. Koyama, Z. Metalkd. **94**, 967 (2003).
[19] A. B. Pippard, in *Magnetoresistance in Metals*, Cambridge studies in Low Temperature Physics Vol. 2 (Cambridge University Press, Cambridge, 1989).
[20] T. Claeson, Phys. Scr. **9**, 353 (1974).
[21] W. L. McMillan, Phys. Rev. **167**, 331 (1968).

[22] Such short Mg-Zn bonds exist in the orthorhombic $Mg_{51}Zn_{20}$ compound (in our VASP calculation, not described here, we used the nearly isostructural but ordered Ag_7Mg_{51}-type structure). Indeed, a simple explanation why the Mg-Zn bonds do not get shorter in the 16 coordinated stoichiometric environment might be that the constraints *between* the 16 atoms (12 of them Zn) forming the shell prevent them from getting closer to the central Mg atom.

[23] G. T. Meaden, *Electrical Resistance of Metals* (Heywood Books, London, 1989).

[24] K. E. Saeger and R. Lück, Phys. Kond. Materie **9**, 91 (1969).

[25] A. Schulte P. Löbl, F. Küβ, and E. Lüscher, J. Phys.: Condens. Matter **4**, 3479 (1992).

[26] T. Matsuda and U. Mizutani, J. Phys. F: Met. Phys. **12**, 1877 (1982).

[27] S. Kashimoto, H. Nakano, Y. Arichika, T. Ishimasa, and S. Matsuo, J. Mater. Sci. Eng. **294-296**, 588 (2000).

[28] Ö. Rapp, in *Physical Properties of Quasicrystals*, edited by Z. Stadnik (Springer-Verlag, Berlin, 1999), Chap. 5.